Momentum-density effects upon the electronic stopping of elemental solids

1999 J. Phys.: Condens. Matter 11 3973

(http://iopscience.iop.org/0953-8984/11/20/304)

J. Phys.: Condens. Matter **11** (1999) 3973–3985. Printed in the UK PII: S0953-8984(99)98449-7

Momentum-density effects upon the electronic stopping of elemental solids

J Wang, Richard J Mathar, S B Trickey and John R Sabin

Quantum Theory Project, Department of Physics, University of Florida, Gainesville, FL 32611-8435, USA

E-mail: trickey@qtp.ufl.edu

Received 15 October 1998, in final form 9 February 1999

Abstract. Treatment of electronic stopping via kinetic theory and the orbital local plasma approximation is extended (from free-standing ordered slabs) to include bulk crystalline targets, and hence probe their electron momentum distribution. Sensitive computational issues, important for comparison with experimental data, are addressed. A primary result is unambiguous first-principles prediction of large gas–solid and film–solid differences in Li stopping. Previous predictions had involved semi-empirical determination of mean excitation energies. Additionally, a stopping anisotropy that is separate from and much smaller than familiar channelling and related to the familiar Compton-profile anisotropy is treated, apparently for the first time. Example calculations for hexagonal Li and graphite are given.

1. Approximate theories of stopping for extended systems

Extensive effort has been devoted to measuring the stopping power (linear energy loss of an energetic charged projectile, or, if normalized to the target density, the stopping cross-section) of elemental systems [1, 2]. Similar effort has been devoted to the theory, calculation and interpretation of stopping [3, 4]. Such calculations are challenging even for the simple case of a proton projectile treated in the first Born approximation. *Without* the Bethe approximation, such a calculation would require that the entire generalized-oscillator-strength (GOS) spectrum be calculated even for the dilute-gas case [3]. In the Bethe approximation [5], the mean excitation energy is meant to be calculated from the dipole oscillator strength distribution (the zero-wavevector GOS distribution). Elsewhere [6], first-principles calculation of the GOS (at levels of refinement beyond the plane-wave Born approximation [7] and with techniques rooted in best practice for prediction of molecular structures) for relevant momentum transfers has been shown to be surprisingly difficult for modern methods even for light isolated atoms. The problem stems from ubiquitous use of finite-basis-set methods (analytical basis) or their finite-numerical-grid equivalents. In the case of an analytical basis, it is easy to see that the calculated GOS must violate the Bethe sum rule at rather low values of momentum transfer. Similar results have been found, unsurprisingly, for the H_2O molecule [8] and other small molecules [9].

The literature on simple dipole oscillator strength distributions even for single atoms makes clear the widespread use of approximate calculations: approximate density functional orbitals in expressions derived for Hartree–Fock wavefunctions, quantum defect orbitals, electron gas models, etc.

0953-8984/99/203973+13$19.50

Treatment of stopping in ordered condensed systems is more demanding than it might seem from this summary. We have developed and currently are using first-principles, *all-electron* codes to calculate the microscopic dielectric function (the analogue for crystals of the GOS). Others have pursued similar *valence-only* calculations [10, 11]. In both cases, these are quite large-scale calculations even for simple elemental targets; hence energy-loss calculations for real material systems of even moderately complicated chemistry and/or geometry are likely to *require* reliable approximate calculations for some time to come.

Proper treatment of shell corrections is another long-standing aspect of stopping cross-section calculations. These corrections may be formulated either in the aggregate (conventionally written as the $C(v)/Z_2$ contribution to the stopping number, with Z_2 the target electron number) or orbital by orbital. The orbital-by-orbital treatment can be developed in terms of orbital mean excitation energies (i.e., orbital partial sums of generalized oscillator strengths or equivalent). That formulation has the advantage of introducing substantially more chemical detail and specificity regarding the target than is provided in a single mean excitation energy. The technique, as we use it, comes from Sabin and Oddershede's [12–14] work on atomic systems; see also [15]. Obviously the challenge of calculation of orbital mean excitation energies also arises for application of this scheme to real condensed systems.

A specific approach to the mean-excitation-energy problem for complex systems is the orbital local plasma approximation (OLPA) [16–18], a generalization of the local plasma approximation (LPA) of Lindhard and Scharff [19]. Essentially the scheme evaluates the logarithm of the plasma frequency of an electron gas at the full electron density at a spatial point, weights that logarithm by the electron density for the specific orbital at that point and integrates. The LPA mean excitation energy is recovered by summing the OLPA mean excitation energies. See below and the extensive literature on the LPA and variants [20].

To predict stopping for ordered films (periodic boundary conditions in two Cartesian directions and vacuum boundary conditions in the third) we used the OLPA with Sigmund's kinetic theory of stopping [21]. Kinetic theory in summary exploits momentum conservation via appropriate Galilean transforms to extend a model of scattering by particles initially at rest to uncorrelated, classical binary collisions involving moving particles. Kinetic theory thus gives stopping for arbitrary projectile velocity via a kinematic integral over the momentum distribution of the target particles multiplied by a stopping factor at the corresponding relative projectile velocity. The momentum distribution can be obtained straightforwardly from an all-electron treatment of the target ground state. For the case of massive particles scattering from that electron distribution, the obvious choice of stopping factor is Bethe stopping (a high-projectile-velocity limiting case). Bethe stopping in conjunction with mean excitation energies in kinetic theory recovers the aggregate shell correction absent in the elementary Bethe stopping formula [12, 22]. Individual shell corrections follow from the use of orbital mean excitation energies; recall the above.

The OLPA coupled with kinetic theory was tested successfully on atoms [17, 18], then applied to ultra-thin films [23, 24], with input quantities from high-precision, all-electron, full-potential calculations in the local spin-density approximation to density functional theory (DFT) [25]. Here we extend the formulation to periodically bounded three-dimensional crystals with a focus on critical technical and computational points, and present results for crystalline lithium (hcp) and graphite as important examples of two phenomena: phase effects and subtle anisotropies in non-channelling proton stopping.

2. Summary of kinetic theory and the OLPA

Kinetic theory plus the OLPA for a crystal is mostly a straightforward extension of the ordered-film version [16]. Here we note the points where there are critical differences while summarizing the notation.

$S(\boldsymbol{v})$ from kinetic theory (equation (19), reference [21]) in Hartree atomic units (used except where noted) is

$$S(\boldsymbol{v}_1) = \int \mathrm{d}^3 v_2 \; f(\boldsymbol{v}_2) \frac{(\boldsymbol{v}_1 + (m/M_1)\boldsymbol{v}_2) \cdot (\boldsymbol{v}_1 - \boldsymbol{v}_2)}{v_1 |\boldsymbol{v}_1 - \boldsymbol{v}_2|} S_0(|\boldsymbol{v}_1 - \boldsymbol{v}_2|) \tag{1}$$

with $\boldsymbol{v}_1$, $\boldsymbol{v}_2$ the projectile ion and target electron velocities respectively, all in the target rest frame. $f(\boldsymbol{v}_2)$ is the normalized velocity distribution of the target electrons. As discussed, S_0 in the Bethe form is used:

$$S_0(v) = \frac{4\pi}{v^2} Z_1^2 Z_2 \theta(2v^2 - I) \ln \frac{2v^2}{I} \tag{2}$$

with Z_1, Z_2 the projectile charge and target electronic charge per scatterer respectively (a homonuclear target is assumed for simplicity), I is the mean excitation energy of the target electron distribution and $\theta(\cdot)$ is the Heaviside unit step function. This expression is valid for $2v^2 > I$ at least. (A more refined approach, beyond the first Born approximation, would include Barkas and Bloch corrections; e.g. equations (96) and (98) in [21].)

Note that the projectile velocity dependence, not just speed, is included, so there are intrinsic anisotropies. The ordered-film calculations did not explore those anisotropies but simply assumed normal incidence to the plane of ordering and simplified the expressions accordingly. Note also that use of a mean-excitation-energy formulation means that only non-channelling anisotropies in the electron distribution can be treated. All impact parameter dependence (equivalently, all dependence on the location of the projectile trajectory on the incident crystalline face) disappears once a treatment based on mean excitation energies is selected. As properties of the electron distribution alone, such energies obviously have no explicit impact parameter or trajectory location dependence.

The original LPA [19] is

$$\ln I = (1/Z_2) \int \mathrm{d}^3 r \; \rho(\boldsymbol{r}) \ln\{\lambda (4\pi \rho(\boldsymbol{r}))^{1/2}\}$$

with $\rho(\boldsymbol{r})$ the electron number density and $\lambda = \sqrt{2}$ an empirical scaling constant. The OLPA extends the prescription in a way that is most physically obvious for a central-field atom. The weighting of the logarithm by the whole density is replaced by the density for the atomic orbital with quantum numbers nl to yield orbital mean excitation energy I_{nl}. (Meltzer *et al* [17, 18] argued that λ should be unity for the OLPA, a choice followed here.)

An equivalent partitioning by orbital labels in extended systems, while not totally obvious, must go consistently to the atomic case in the limit of arbitrarily large lattice spacings. A simple choice (used previously with the slabs) which does so is to partition the occupied Kohn–Sham (KS) eigenvalues into ranges. Thus, if the occupied KS bands are between $\varepsilon_{\min}$ and ε_F (with ε_F the Fermi energy), then W energy ranges are defined as

$$\varepsilon_l = \varepsilon_{\min} + (l-1) \frac{\varepsilon_F - \varepsilon_{\min}}{W} \qquad l = 1, \ldots, W+1. \tag{3}$$

The approximate orbital mean excitation energy for each range then is

$$\ln I_l = \frac{1}{\eta_l} \int_\Omega \mathrm{d}^3 r \; \rho_l(\boldsymbol{r}) \ln\{(4\pi \rho(\boldsymbol{r}))^{1/2}\} \tag{4}$$

where Ω is the unit-cell volume, $\rho_l(\boldsymbol{r})$ is the electron number density associated with the KS eigenvalues in the range l, η_l is the number of electrons with KS eigenvalues in that range

$$\eta_l = \int_\Omega \mathrm{d}^3 r\ \rho_l(\boldsymbol{r})$$

and the total number of electrons per unit cell is

$$\sum_l \eta_l = Z_{\mathrm{cell}}.$$

The partitioning in (4) has the proper separated-atom limit (mentioned above) if the ranges bracket bands of appropriate symmetry. It also ensures that the sum of the I_l is the LPA I. Details are in [18].

Correspondingly the Bethe stopping number for range l is $L_l(v) = \ln[2v^2/I_l]$ and the resulting kinetic stopping is

$$S(\boldsymbol{v}) = \sum_l S_l(\boldsymbol{v})$$

$$\equiv 4\pi Z_1^2 Z_2 \sum_l \int \mathrm{d}^3 v_2\ f_l(\boldsymbol{v}_2) L_l(|\boldsymbol{v}_1 - \boldsymbol{v}_2|) \frac{(\boldsymbol{v}_1 + (m/M_1)\boldsymbol{v}_2) \cdot (\boldsymbol{v}_1 - \boldsymbol{v}_2)}{v_1 |\boldsymbol{v}_1 - \boldsymbol{v}_2|^3} \qquad (5)$$

with $f_l(\boldsymbol{v}_2)$ the electron momentum (velocity) density for KS states with energies in the range l. Note that (5) preserves the explicit dependence on projectile velocity. For proton projectiles, m/M_1 is small and will be dropped.

3. Electron momentum density

Reliable, rapid calculation of $S(\boldsymbol{v})$s for complicated crystals from (5) depends upon quick, accurate generation of $\rho_l(\boldsymbol{r})$ and $f_l(\boldsymbol{v}_2)$ plus rapid integration over momentum (velocity). The underlying DFT solutions were obtained from a precise, efficient, all-electron, full-potential code, namely the linear combination of Gaussian-type orbitals with fitting functions methodology (LCGTO–FF) [26] code GTOFF [27]. All-electron methodology together with orbital mean excitation energies gives stopping contributions from each band on an equal footing (as distinct from pseudopotential treatments of extended systems), thereby allowing such subtleties as surface–core-level shift effects to be probed. Full-potential methodology ensures that any calculated projectile-direction anisotropies are actually in the physical model and not procedural artifacts.

The LCGTO solution of the KS equation involves Bloch-symmetrized Gaussian basis functions $\phi_j(\boldsymbol{r}, \boldsymbol{k})$ for each contracted Gaussian function χ_j of type j at point $\boldsymbol{k}$:

$$\phi_j(\boldsymbol{r}, \boldsymbol{k}) = \frac{1}{\sqrt{N_{\mathrm{cell}}}} \sum_{\boldsymbol{R}} \exp(\mathrm{i}\boldsymbol{k} \cdot \boldsymbol{R}) \chi_j(\boldsymbol{r} + \boldsymbol{R}) \qquad (6)$$

(Note: the vectors $\boldsymbol{k}$ are three or two dimensional depending on whether the ordered system is a crystal or a slab (ordered film). Both the electron density and the vectors $\boldsymbol{r}$ are three dimensional, so for slabs the two-dimensional wavevectors are embedded in 3-space.) The KS orbitals $\varphi_{i,\boldsymbol{k}}(\boldsymbol{r})$ for band i at Brillouin zone (BZ) point $\boldsymbol{k}$ are linear combinations of the Bloch basis functions

$$\varphi_{i,\boldsymbol{k}}(\boldsymbol{r}) = \sum_j C_{ji}(\boldsymbol{k}) \phi_j(\boldsymbol{r}, \boldsymbol{k}) \qquad (7)$$

whence

$$\rho_l(\boldsymbol{r}) = \sum_{i,\boldsymbol{k}} n_{i,\boldsymbol{k}} \left|\varphi_{i,\boldsymbol{k}}(\boldsymbol{r})\right|^2 [\theta(\varepsilon_{l+1} - \epsilon_{i,\boldsymbol{k}}) - \theta(\varepsilon_l - \epsilon_{i,\boldsymbol{k}})] \qquad (8)$$

with $n_{i,\boldsymbol{k}}$ the occupancy for band i at BZ point $\boldsymbol{k}$.

With omission of the Lam–Platzman correction [28] the momentum density for range l is

$$\rho_l(\boldsymbol{v}) = \sum_{i,\boldsymbol{k}} n_{i,\boldsymbol{k}} \left|\varphi_{i,\boldsymbol{k}}(\boldsymbol{v})\right|^2 [\theta(\varepsilon_{l+1} - \epsilon_{i,\boldsymbol{k}}) - \theta(\varepsilon_l - \epsilon_{i,\boldsymbol{k}})]$$

with the Fourier transform of the KS orbitals given by

$$\varphi_{i,\boldsymbol{k}}(\boldsymbol{v}) = \frac{1}{\sqrt{N_{\text{cell}}\Omega}} \int \mathrm{d}^3 r \ \exp(\mathrm{i}\boldsymbol{v}\cdot\boldsymbol{r})\varphi_{i,\boldsymbol{k}}(\boldsymbol{r}). \tag{9}$$

N_{cell} is the total number of unit cells in the crystalline periodic volume; for slabs there is a factor of 2π in the denominator and Ω refers to a two-dimensional unit cell [16]. Equations (6), (7) and (9) then give

$$\rho_l(\boldsymbol{v}) = \frac{1}{\Omega} \sum_i n_{i,\tilde{\boldsymbol{v}}} \left[\theta(\varepsilon_{l+1} - \epsilon_{i,\tilde{\boldsymbol{v}}}) - \theta(\varepsilon_l - \epsilon_{i,\tilde{\boldsymbol{v}}})\right] \left| \sum_j C_{ji}(\tilde{\boldsymbol{v}}) \int \mathrm{d}^3 r \ \exp(\mathrm{i}\boldsymbol{v}\cdot\boldsymbol{r})\chi_j(\boldsymbol{r}) \right|^2 \tag{10}$$

where $\tilde{\boldsymbol{v}}$ is $\boldsymbol{v}$ reduced to the first BZ. The velocity distribution function $f_l(\boldsymbol{v})$ in (1) and (5) is simply

$$f_l(\boldsymbol{v}) = \rho_l(\boldsymbol{v})/Z_{\text{cell}}.$$

In principle, both $\boldsymbol{v}$ and $\boldsymbol{k}$ are continuous. Translational symmetry, manifest in $\tilde{\boldsymbol{v}}$ (which comes from $\delta_{\boldsymbol{v},\boldsymbol{k}+\boldsymbol{K}}$), forces them to be related on the reciprocal-space lattice. As is customary with periodic systems, GTOFF solves the KS equations on a separate mesh in the first BZ (or its irreducible wedge, IBZ); $\boldsymbol{k}$ becomes a discrete variable. The mesh and associated weights for BZ zone integrals are chosen by a well-known scheme [29]. The combination of these two discrete meshes results in the integration over $\boldsymbol{v}_2$ in (5) being reduced in the crystalline case to summation over a discrete mesh in the first BZ displaced by each $\boldsymbol{K}$. For the periodic films, integration over the direction normal to the two-dimensional BZ remains.

To utilize quantities calculated (in GTOFF) on the mesh $\boldsymbol{k}_i$ (and associated weights) correctly in the evaluation of the velocity integral in (5), the projectile velocity vector must be treated explicitly. Its orientation has no *a priori* relationship with the reciprocal-space symmetries. As is evident from the kinematic factor $\boldsymbol{v}_1 \cdot (\boldsymbol{v}_1 - \boldsymbol{v}_2)$ in (5), the forward and backward points $+\boldsymbol{v}_2$ and $-\boldsymbol{v}_2$ contribute differently for stopping, even though they are equivalent in the solution of the KS equations on the BZ mesh for those cases in which the reciprocal lattice has a mirror plane perpendicular to the ion direction. Evaluation of (5) therefore in general requires knowledge of solutions to the KS equation on a larger set of $\boldsymbol{k}$-points than the set which normally is sampled in the IBZ while solving the KS equations.

A direct but uneconomical remedy would be to treat all of the necessary $\boldsymbol{k}$-points compatible with the symmetry of the integrand of (5) with respect to $\boldsymbol{v}$. Group theory provides the needed alternative straightforwardly. Consider the effect of O, a member of the isogonal point group of the system, operating on the Fourier transform of the KS eigenfunction $\varphi_{i,\boldsymbol{k}}$:

$$\begin{aligned}
\varphi_{i,\boldsymbol{k}}(O^{-1}\boldsymbol{v}) &= \frac{1}{\sqrt{\Omega N_{\text{cell}}}} \int \mathrm{d}^3 r \ \exp(\mathrm{i}O^{-1}\boldsymbol{v}\cdot\boldsymbol{r})\varphi_{i,\boldsymbol{k}}(\boldsymbol{r}) \\
&= \frac{1}{\sqrt{\Omega N_{\text{cell}}}} \int \mathrm{d}^3 r' \ \exp(\mathrm{i}\boldsymbol{v}\cdot\boldsymbol{r}')\varphi_{i,\boldsymbol{k}}(O^{-1}\boldsymbol{r}') \\
&= \frac{1}{\sqrt{\Omega N_{\text{cell}}}} \int \mathrm{d}^3 r \ \exp(\mathrm{i}\boldsymbol{v}\cdot\boldsymbol{r})O\varphi_{i,\boldsymbol{k}}(\boldsymbol{r}) \\
&= \frac{1}{\sqrt{\Omega N_{\text{cell}}}} \int \mathrm{d}^3 r \ \exp(\mathrm{i}\boldsymbol{v}\cdot\boldsymbol{r})\varphi'_{i,O\boldsymbol{k}}(\boldsymbol{r}).
\end{aligned}$$

The last step is justified because operating on $\varphi_{i,\boldsymbol{k}}(\boldsymbol{r})$ with O produces an eigenfunction in Bloch form with $\boldsymbol{k}$ rotated by $O\boldsymbol{k}$ at the same energy [30]. In the usual case of no degeneracy, $\varphi_{i,\boldsymbol{k}}(\boldsymbol{r})$ and $\varphi'_{i,\boldsymbol{k}}(\boldsymbol{r})$ can differ at most by a phase factor, whence

$$\rho_{i,O\boldsymbol{k}}(\boldsymbol{v}) = \rho_{i,\boldsymbol{k}}(O^{-1}\boldsymbol{v}).$$

For degeneracies, $\varphi_{i,\boldsymbol{k}}(\boldsymbol{r})$ and $\varphi'_{i,\boldsymbol{k}}(\boldsymbol{r})$ are related by a unitary transform in the degenerate subspace

$$\varphi'_{l,\boldsymbol{k}}(\boldsymbol{r}) = \sum_m \Gamma_{l,m}\varphi_{m,\boldsymbol{k}}(\boldsymbol{r})$$

where l, m index the degenerate bands. Then one has

$$\sum_l \rho_{l,O\boldsymbol{k}}(\boldsymbol{v}) = \sum_m \rho_{m,\boldsymbol{k}}(O^{-1}\boldsymbol{v})$$

because Γ is unitary. The OLPA energy ranges allow degenerate bands at a particular energy to be summed in a single range, so beyond that degenerate bands require no particular special treatment. These symmetry considerations reduce the information needed for calculation of the electron momentum density to only that found in the IBZ. Additional symmetry with respect to the projectile trajectory, if any, of course could be exploited to reduce further the number of different $\boldsymbol{k} + \boldsymbol{K}$ points included in the calculation of the momentum-space integral.

By contrast, recall that the prior work on ordered-film stopping [23] assumed the axis defined by the projectile velocity to be normal to the film BZ. Such a special axis introduces no symmetry constraint with respect to the film layer group (2-D space group).

Further computational speed (compared to the prior implementation [23, 24]) comes from analytical Fourier transforms. GTOFF uses Hermite Gaussian basis functions (χ_j in (10)):

$$\chi_{n\alpha}(\boldsymbol{r}) = N_{n\alpha}\frac{\partial^{n_1}}{\partial A_x^{n_1}}\frac{\partial^{n_2}}{\partial A_y^{n_2}}\frac{\partial^{n_3}}{\partial A_z^{n_3}}\exp(-\alpha\,|\boldsymbol{r}-\boldsymbol{A}|^2)$$

where $\boldsymbol{A}$ is the centre of the Gaussian and $N_{n\alpha}$ a normalization constant [31]. The analytical Fourier transform is

$$\int \chi_{n\alpha}(\boldsymbol{r})\exp(\mathrm{i}\boldsymbol{v}\cdot\boldsymbol{r})\,\mathrm{d}^3r = N_{n\alpha}\left(\frac{\pi}{\alpha}\right)^{3/2} v_x^{n_1}v_y^{n_2}v_z^{n_3}\mathrm{i}^{n_1+n_2+n_3}\exp\left(\mathrm{i}\boldsymbol{v}\cdot\boldsymbol{A}-\frac{v^2}{4\alpha}\right).$$

4. Results: phase effects, anisotropy

4.1. Lithium films and hcp lithium

An entirely new stopping code was written to implement these extensions and technical improvements, then checked against the previous hexagonal H and Li N-layer OLPA calculations [23, 24]. Table 1 and figure 1 provide a brief comparison of the two calculations for Li. (Compare figure 1 with figure 1 in [24].) The N-layer lattice parameters and basis sets were taken from [24, 32]. The hcp solid lattice parameters were from Nobel *et al* [33], while the basis sets for the solid were constructed by taking the functions for only the inner, solid-like layers of the N-layer sets in reference [32].

The present calculations, for both crystals and atoms, differ from the prior ones in important ways. The earlier atomic stopping results were for isolated central-field atoms [18]. The present atomic values actually are quasi-atomic: they were calculated by expanding the lattice spacing of the 1-layer to $a = 15$ au. This procedure has the advantage of using the same code for all results. More importantly, the previous solid results were determined semi-empirically by Sabin and Oddershede [14]. They treated the mean excitation energies as quasi-atomic

Table 1. Mean excitation energies I in eV, peak values of the stopping cross section in units of 10^{-15} eV cm^2 per atom and velocity (in au) at which that maximum occurs for Li N-layers, hcp Li and dilute-gas (atomic) stopping. See the text regarding differences in calculational methods for prior values [24].

Quantity	Atom	$N=1$	$N=2$	$N=3$	$N=4$	Crystal
I_1						
Present	71.54	71.88	72.04	72.07	72.11	72.14
Prior	71.48	71.93	72.07	72.07	72.11	109.32
I_2						
Present	3.21	7.08	8.33	8.76	9.12	9.66
Prior	3.42	7.12	8.38	8.92	9.19	10.46
$I_{\rm tot}$						
Present	25.25	34.19	36.18	36.78	37.34	37.55
Prior	25.94	33.25	35.16	35.93	36.29	50.0
$S_{\rm max}$						
Present	38.78	19.25	16.34	15.68	15.08	14.24
Prior	35.57	19.06	16.00	15.15	14.83	12.72
$v_{\rm max}$						
Present	0.54	0.79	0.86	0.88	0.89	0.96
Prior	0.55	0.77	0.90	0.96	0.98	0.99

quantities, with I_{1s} extracted from published atomic calculations [34] and I_{2s} from fitting the isotropic kinetic stopping theory to the tabulated [2] high-energy stopping data. The electron momentum distribution they derived from experimental isotropic Compton-profile data for polycrystalline Li.

Extension of OLPA kinetic stopping to treatment of bulk crystals makes possible the first check of that earlier semi-empirical work entirely independently of experiment. Table 1 shows that the values of I_1, the 1s-band mean excitation energy, differ substantially. The deficiency in core-level mean excitation energies is intrinsic to OLPA, since it shows up even for isolated atoms [17]. In contrast, the semi-empirical and OLPA values for the valence band mean excitation energy I_2 differ very little. Therefore the difference between the present and previous calculated crystalline stopping must arise primarily from the discrepancy in the 1s-band I. Other contributions to the difference (use of two different momentum distributions, polycrystallinity in the semi-empirical value) are likely to be small. This appraisal is supported by the fact that for proton velocities $\geqslant 2$ au, where projectile charge-state effects are known experimentally to be negligible, the calculated crystalline stopping lies a few per cent above the measured [35] values (too close to be shown easily in figure 1). If the ratio of the KS and measured K-shell energies for Li is used to scale the calculated I_{1s} and Bethe logarithm, however, agreement is achieved.

Thus the first new result of this work is purely first-principles confirmation of the very large gas–solid phase effect for Li stopping previously predicted by Sabin and co-workers [14, 36]. The present prediction of the ratio of stopping maxima (atom/crystal) is 2.7 while the prior work [14] found 2.9. The predicted positions of those maxima are altered by less than 4% at most.

Overall the agreement between the present and prior OLPA calculations is quite reasonable. None of the published conclusions is altered by the differences. In particular, the $1/N$ linear

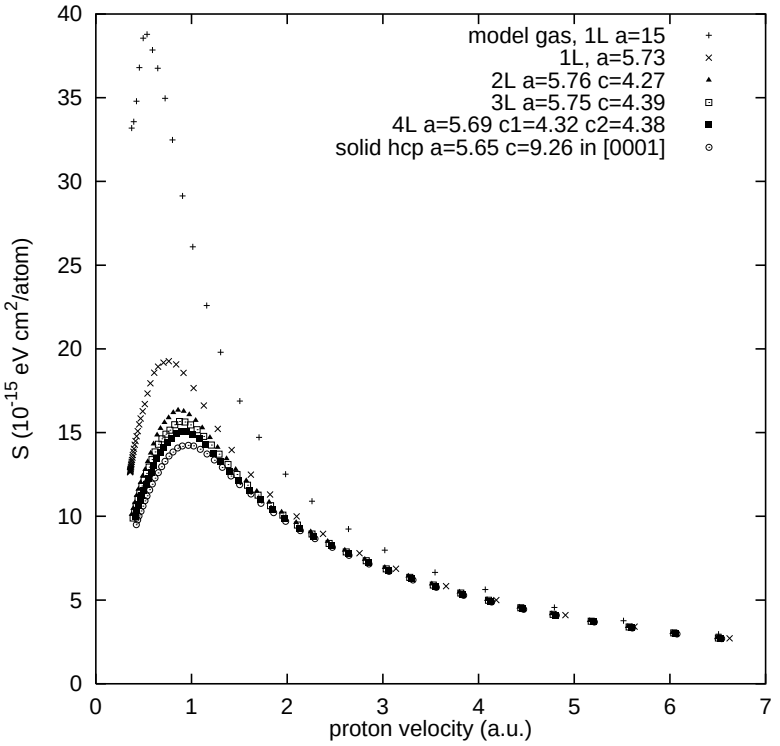

Figure 1. Comparison of proton stopping for hexagonal Li N-layers, the hcp solid and the isolated atom in units of 10^{-15} eV cm^2 per atom. Normal incidence for the N-layers; [0001] incidence for the crystal. The present calculation for the bulk uses the theoretical K-shell energy of -45 eV, whereas the experimental energy is -55 eV. A correction (scaling) of the theoretical I-value by the ratio of these values and further scaling with the Bethe logarithm (2) explains the slight overestimation of the experimental stopping [35] by about 4.7% at $v = 5$ au.

scaling for convergence of the layers toward the bulk value [37]

$$S(N, v) = S(\infty, v) + \frac{1}{N} S_L(v) \tag{11}$$

found earlier remains valid. The constant-coefficient values differ by 2% or less and all but one of the values of $S_L(v)$ behave similarly; see table 2 for values at selected projectile velocities. (Corresponding conclusions hold for the H N-layers, so those results are not tabulated here.) The observed changes are consistent with being the cumulative result of refinements in numerical techniques (both from FILMS to GTOFF and in the previous versus new implementations of the kinetic OLPA).

We turn to directional dependences. The anisotropy of electronic stopping with respect to projectile incidence direction, channelling, has been the subject of much study [38]. Channelling calculations frequently utilize potential models ('string' potentials) or equivalent assumptions about sampling the relatively diffuse electron charge density along and near the channel axis. Such approaches select, implicitly or explicitly, a particular range of impact parameters (measured from the channel central axis); see for example reference [39]. Anisotropy of this kind, which is associated with the specific location of the projectile trajectory in the unit cell, is intrinsically inaccessible to a mean-excitation-number formulation, as already remarked.

Table 2. Coefficients of the linear fit in $1/N$, equation (11), in units of 10^{-15} eV cm^2 per atom.

Quantity	v (au)	$S(\infty, v)$	$S_L(v)$
Present	1.25	13.23	2.23
Prior [37]		13.00	2.32
Present	1.75	10.64	1.02
Prior [37]		10.53	1.11
Present	2.50	8.02	0.53
Prior [37]		7.95	0.53
Present	4.00	5.07	0.20
Prior [37]		5.05	0.21
Present	6.00	3.04	0.09
Prior [37]		3.02	0.09

A distinct (but related) issue is the cumulative anisotropy for all possible impact parameters, as for example in the recent simulation by van Dijk *et al* [40] and related work on the inverse first velocity moment of $S(\boldsymbol{v})$ by Tielens *et al* [41] both for Si. Consider two directions, including inequivalent high-symmetry ones. If all target electrons could be probed on an equal footing, and hence be selected (as collision partners) without the preference given to diffuse (valence) states during channelling, whatever stopping anisotropy resulted would be the least possible for that pair of directions. Call this the minimum stopping anisotropy (MSA). Closely related physics is the stopping anisotropy related to principal axes in orientable molecules modelled by Apell *et al* [42] via jellium ellipsoids and treated earlier by Sauer *et al* [43] by polarization propagator calculations of directionally dependent mean excitation energies.

Equation (5) shows that the MSA will occur for any system without the symmetry of the full rotation group, e.g. molecules, slabs and solids. (For atomic stopping the effect disappears *a priori* (cf. e.g. reference [4]), on averaging over rotational orientations, since the same rotational averaging occurs in a dilute-gas sample.) Another kind of closely related physics is in the anisotropic Compton profiles; in both cases, the source of the anisotropy is the electron momentum-density topology. That source also highlights the distinction from channelling. The momentum-space formulation (1) implies complete absence of the knowledge of the real-space location of the ion–electron scattering events. (This characteristic is similar to employing only the macroscopic element of the inverse dielectric matrix in the dielectric *ansatz* [10, 41].) Because of that absence, the MSA reflects the point group symmetry of the Bravais lattice [44] in terms of directional dependencies and the integrated effects of bonding upon the scattering charge distribution. It does not probe the specific atomic site information as would be required (explicitly or implicitly) for a full microscopic treatment of the channelling phenomenon (atomic strings, channel centres, dechannelling, etc).

The hcp Li bulk stopping results for table 1 are for protons incident along [0001]. The calculated MSA magnitude is potentially relevant in at least three ways. Is the MSA in Li large enough to alter the confirmation of predicted phase effects? Is the use of an expanded-lattice crystal (or ordered film) to model the gas-phase stopping legitimate? Is the comparison between calculated and semi-empirical Li crystalline stopping altered substantively by averaging the new crystalline results over orientations?

Figure 2 shows the calculated MSA as a difference in hcp solid Li for directions $\boldsymbol{v}_{[0001]}$

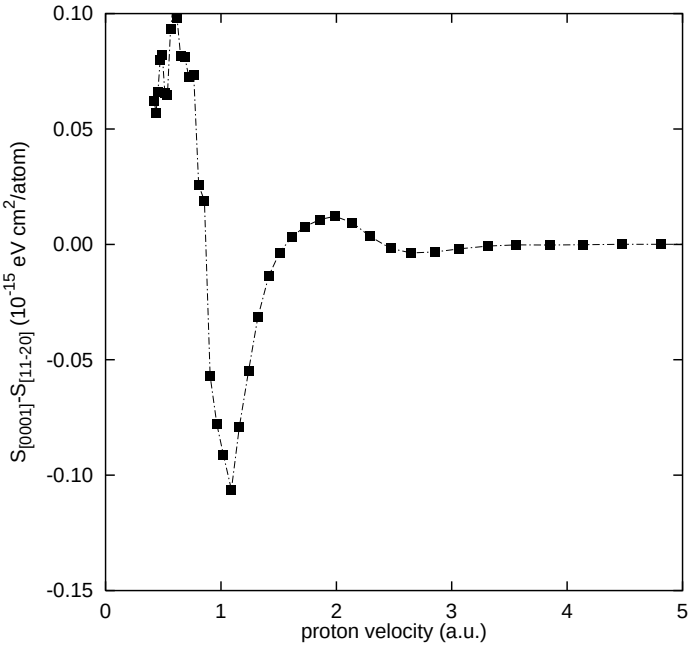

Figure 2. The MSA for protons on hcp solid Li, in units of 10^{-15} eV cm^2 per atom, for directions [0001] versus [11$\bar{2}$0].

and $\boldsymbol{v}_{[11\bar{2}0]}$, namely

$$S(\boldsymbol{v}_{[0001]}) - S(\boldsymbol{v}_{[11\bar{2}0]}).$$

(The small fluctuations below $v = 2$ au are ignorable numerical artifacts.) The MSA is less than 1%, much smaller than the predicted 270% phase effect difference. It also is much too small to alter the comparison between first-principles and semi-empirical results or to make use of an expanded 1-layer as a proxy for a truly isolated, isotropic Li atom an unreliable practice.

4.2. Graphite

An interesting and much-studied case of highly anisotropic chemical bonding is graphite. Because of the dominance of π-electron bonding in graphite, a significant anisotropy for $\boldsymbol{q}$ parallel versus perpendicular to the c-axis is expected. Such anisotropy is seen experimentally in the Compton profile [45, 46]. Figure 3 shows the calculated proton stopping curves in the direction [0001] for equilibrium graphite. Lattice parameters and basis sets are from the recent GTOFF calculation by Boettger [47]. Figure 4 gives the MSA difference curve. Compared with the Li results of figure 2, the main difference is in the low-energy region where the projectile velocity is comparable to the orbital velocity of the target electrons. In graphite, the [11$\bar{2}$0] stopping dominates over that for [0001], with the converse situation in hcp Li. The size of the MSA reaches about 1%, which is of the same order as the anisotropy in the Compton profile [45]. Indeed, this difference curve has a strong qualitative resemblance to the observed Compton-profile difference curve of figure 2 in Tyk *et al* [45], clearly suggestive of their common physical origin in the electron momentum density. Once again the small fluctuations below $v = 2$ au are ignorable numerical artifacts.

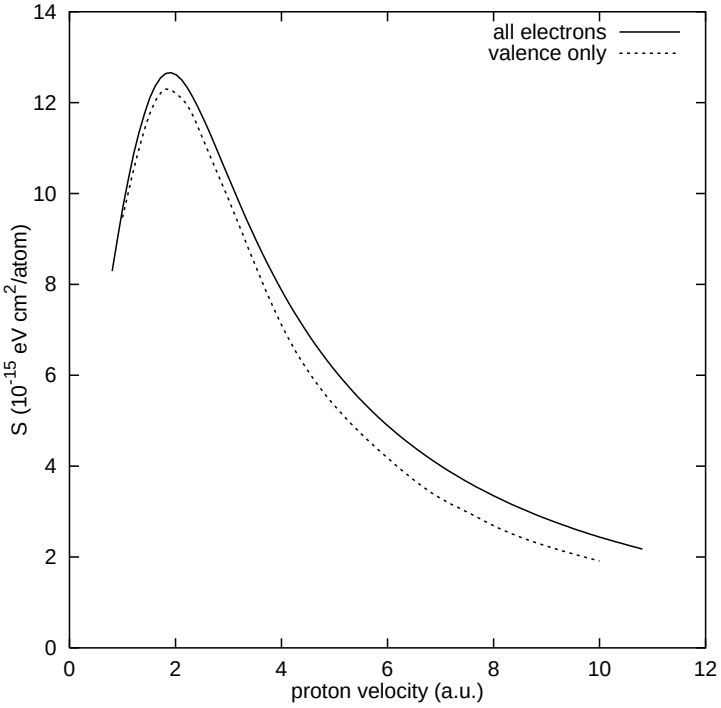

Figure 3. Proton stopping for solid graphite, in units of 10^{-15} eV cm^2 per atom, in direction [0001].

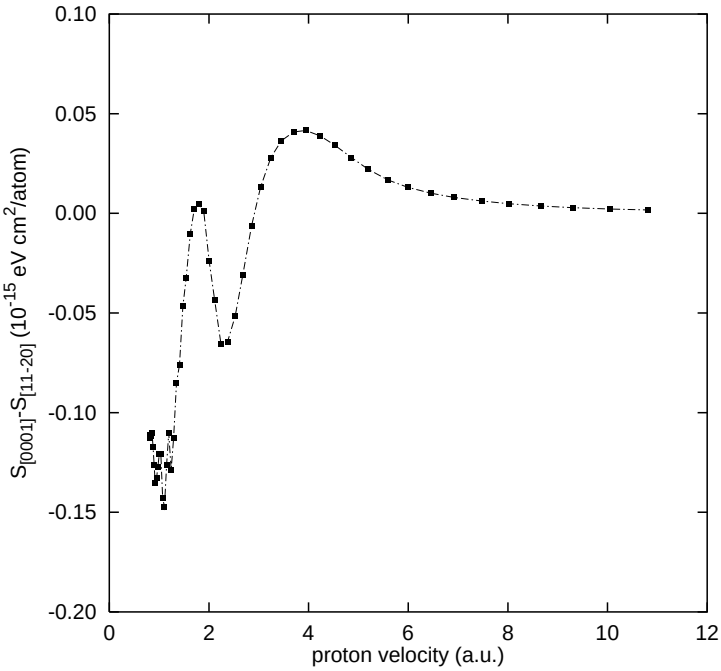

Figure 4. The MSA for protons on solid graphite, in units of 10^{-15} eV cm^2 per atom, for directions [0001] versus [11$\bar{2}$0].

The MSA would be expected to arise primarily from valence electrons. Within the kinetic theory limitations regarding real-space location of the scattering events already discussed, the most that can be done to assess the relative importance of valence contributions is to compare the valence-only and all-electron stopping anisotropies. As figure 3 shows, the dominant effect of removing the core is a simple shift downward of $S(v)$. Unsurprisingly, that shift is essentially isotropic; were we to plot the valence-only version of figure 4 the result would be virtually indistinguishable. We therefore venture a somewhat more speculative remark. The contribution of the nuclear energy loss is small compared to the electronic energy loss at the intermediate and high energies considered here. It is also smaller under channelling conditions than for the 'random' case. Therefore the anisotropy in channelling stopping should be proportional to the valence MSA [48].

In summary, we have extended the OLPA and kinetic theory treatment of electronic stopping to crystalline targets, re-implemented the methodology in a more efficient and general code and used the new code to confirm the predicted strong phase effect in Li without reliance on experimental inputs and to predict minimum stopping anisotropies for graphite.

Acknowledgments

We thank J Z Wu and J C Boettger for helpful conversations and access to unpublished results. Support from the US Army Research Office (Award DAAH04-95-1-0326) is gratefully acknowledged.

References

[1] Andersen H H and Ziegler J F 1977 *Stopping Powers and Ranges in All Elements* (New York: Pergamon)
[2] Janni J F 1982 *At. Data Nucl. Data Tables* **27** 341–529
[3] Fano U and Rau A R P 1986 *Atomic Collisions and Spectra* (New York: Academic)
[4] Inokuti M 1971 *Rev. Mod. Phys.* **43** 297–347
Inokuti M, Hikawa Y and Turner J E 1978 *Rev. Mod. Phys.* **50** 23–35
[5] Bethe H A 1930 *Ann. Phys., Lpz.* **5** 325
[6] Mortensen E H, Oddershede J and Sabin J R 1992 *Nucl. Instrum. Methods* B **69** 24–32
Nobel J A, Oddershede J, Sabin J R and Trickey S B 1994 *15th Werner Brandt Workshop (Gainesville, FL)* pp 83–99 unpublished
[7] For example, see
McGuire E J 1998 *Phys. Rev.* A **57** 2758–71
[8] Durante N, Lamanna U T, Arrighini G P and Guidotti C 1995 *Theor. Chim. Acta* **90** 115–34
[9] Oddershede J and Sabin J R 1998 *Polish J. Chem.* **72** 1376–88
[10] Mathar R J, Trickey S B and Sabin J R 1997 *17th Werner Brandt Workshop (Charlottesville, VA)* pp 11–18 unpublished
Mathar R J, Sabin J R and Trickey S B 1999 *Nucl. Instrum. Methods* B at press
[11] Pitarke J M, Campillo I, Eguiluz A G and García A 1997 *17th Werner Brandt Workshop (Charlottesville, VA)* (unpublished)
Campillo I, Pitarke J M, Eguiluz A G and García A 1998 *Nucl. Instrum. Methods* B **135** 103–6
[12] Sabin J R and Oddershede J 1982 *Phys. Rev.* A **26** 3209–19
Sabin J R and Oddershede J 1984 *Phys. Rev.* A **29** 1757–62
[13] Oddershede J and Sabin J R 1984 *At. Data Nucl. Data Tables* **31** 275–97
[14] Sabin J R and Oddershede J 1989 *Nucl. Instrum. Methods* B **36** 249–53
[15] Pathak A 1975 *Phys. Status Solidi* b **71** K35–8
[16] Trickey S B, Wu J Z and Sabin J R 1994 *Nucl. Instrum. Methods* B **93** 186–94
[17] Meltzer D E, Sabin J R and Trickey S B 1990 *Phys. Rev.* A **41** 220–32
Meltzer D E, Sabin J R and Trickey S B 1990 *Phys. Rev.* A **42** 666 (erratum)
[18] Meltzer D E, Sabin J R, Trickey S B and Wu J Z 1993 *Nucl. Instrum. Methods* B **82** 493–502
[19] Lindhard J and Scharff M 1953 *K. Dansk. Vidensk. Selsk. Mat.-Fys. Medd.* **27** No 15

Lindhard J and Scharff M 1960 *Report on Conference on Penetration of Atomic Particles (Gatlinburg, 1958) Natl Acad. Sci.—Natl Res. Council, Publication* 752, section II-1
[20] For example, see
Rousseau C C, Chu W K and Powers D 1971 *Phys. Rev.* A **4** 1066–70
Johnson R E and Inokuti M 1983 *Comment. At. Mol. Phys* **14** 19–31
Tung C J and Watt D E 1985 *Radiat. Eff.* **90** 177–90
Balashova L L, Chumanova O V and Kabachnik N M 1989 *Phys. Status Solidi* b **155** 289–94
Cabrera-Trujillo R, Cruz S A and Soullard J 1994 *Nucl. Instrum. Methods* B **93** 166–74
[21] Sigmund P 1982 *Phys. Rev.* A **26** 2497–517
[22] Sigmund P and Haagerup U 1986 *Phys. Rev.* A **34** 892–910
[23] Wu J Z, Trickey S B, Sabin J R and Meltzer D E 1991 *Nucl. Instrum. Methods* B **56+57** 340–4
[24] Wu J Z, Trickey S B and Sabin J R 1993 *Nucl. Instrum. Methods* B **79** 206–9
[25] Kohn W and Sham L J 1965 *Phys. Rev.* **140** A1133–8
[26] Boettger J C and Trickey S B 1985 *Phys. Rev.* B **32** 1356–8
Mintmire J W, Sabin J R and Trickey S B 1982 *Phys. Rev.* B **26** 1743–53
Birkenheuer U, Boettger J C and Rösch N 1994 *J. Chem. Phys.* **100** 6826–36
[27] Boettger J C 1995 *Int. J. Quantum Chem., Quantum Chem. Symp.* **29** 197–202
Boettger J C and Trickey S B 1996 *Phys. Rev.* B **53** 3007–12
[28] Lam L and Platzman P M 1974 *Phys. Rev.* B **9** 5122–7
Bauer G E W 1983 *Phys. Rev.* B **27** 5912–8
Görling A, Levy M and Perdew J P 1993 *Phys. Rev.* B **47** 1167–73
[29] Monkhorst H J and Pack J D 1976 *Phys. Rev.* B **13** 5188–92
Blöchl P E, Jepsen O and Andersen O K 1994 *Phys. Rev.* B **49** 16 223–33
[30] Tinkham M 1964 *Group Theory and Quantum Mechanics* (New York: McGraw-Hill) p 279
[31] Živković T and Maksić Z B 1968 *J. Chem. Phys.* **49** 3083–7
[32] Boettger J C and Trickey S B 1992 *Phys. Rev.* B **45** 1363–72
[33] Nobel J A, Trickey S B, Blaha P and Schwarz K 1992 *Phys. Rev.* B **45** 5012–4
[34] Dehmer J L, Inokuti M and Saxon R P 1975 *Phys. Rev.* A **12** 102–21
[35] Eppacher Ch, Díez Muiño R, Semrad D and Arnau A 1995 *Nucl. Instrum. Methods* B **96** 639–42
[36] Oddershede J, Sabin J R and Sigmund P 1983 *Phys. Rev. Lett.* **51** 1332–5
[37] Apell S P, Sabin J R and Trickey S B 1995 *Int. J. Quantum Chem., Quantum Chem. Symp.* **29** 153–9
Apell S P, Sabin J R and Trickey S B 1997 *Phys. Rev.* A **56** 3769–76
[38] For example:
Kumakhov M A and Komarov F F 1981 *Energy Loss and Ion Ranges in Solids* (translated by B Teague) (New York: Gordon and Breach) ch 3
Nastasi M, Mayer J W and Hirvonen J K 1996 *Ion–Solid Interactions* (Cambridge: Cambridge University Press) ch 6
Nobel J A, Sabin J R and Trickey S B 1995 *Nucl. Instrum. Methods* B **99** 632, references 3–13
[39] Dettmann K 1975 *Z. Phys.* A **272** 227–35
[40] van Dijk P W L, van Ijzendoorn L J, de Koning M, Bobbert P, van Haeringen W and de Voigt M J A 1994 *Nucl. Instrum. Methods* B **85** 551–5
[41] Tielens T M H E, Bauer G E W and Stoof T H 1994 *Phys. Rev.* B **49** 5741–4
[42] Apell S P, Trickey S B and Sabin J R 1998 *Phys. Rev.* A **58** 4616–21
[43] Sauer S P A, Sabin J R and Oddershede J 1995 *Nucl. Instrum. Methods* B **100** 458–63
[44] Nye J F 1957 *Physical Properties of Crystals* (Oxford: Clarendon)
[45] Tyk R, Felsteiner J, Gertner I and Moreh R 1985 *Phys. Rev.* B **32** 2625–7
[46] Manninen S, Honkimaki V and Suortti P 1992 *J. Appl. Crystallogr.* **25** 268–73
[47] Dunlap B I and Boettger J C 1996 *J. Phys. B: At. Mol. Phys.* **29** 4907–13
Boettger J C 1997 *Phys. Rev.* B **55** 11 202–11
[48] Eriksson L, Davies J A and Jespersgaard P 1967 *Phys. Rev.* **161** 219–34
Eriksson L 1967 *Phys. Rev.* **161** 235–44